Optical Sensors for Process Control and Emissions Monitoring in Industry

Sarah W. Allendorf, David K. Ottesen, David W. Hahn, Tom J. Kulp and Uta B. Goers

Sandia National Laboratories, MS 9052, Livermore CA 94551

ABSTRACT

Laser-based sensors, currently under development and testing at Sandia National Laboratories for process control, emissions monitoring, and pollution prevention, are discussed.

Keywords: tunable diode laser, spectroscopy, laser spark spectroscopy, periodically-poled lithium niobate, steelmaking, incineration, continuous emissions monitors, process control

1. INTRODUCTION

Sandia National Laboratories has a number of ongoing projects developing optical sensors for industrial environments. Laser-based sensors can be attractive for relatively harsh environments where extractive sampling is difficult, inaccurate, or impractical. Tools developed primarily for laboratory research can often be adapted for the "real world" and applied to problems far from their original uses. Spectroscopic techniques, appropriately selected, have the potential to impact the bottom of line of a number of industries and industrial processes.

In this paper we discuss three such applications: a laser-based instrument for process control in steelmaking, a laser-induced breakdown method for hazardous metal detection in process streams, and a laser-based imaging sensor for evaluating surface cleanliness. Each has the potential to provide critical, process-related information in a real-time, continuous manner. These sensor techniques encompass process control applications and emissions monitoring for pollution prevention. They also span the range from a field-tested pre-commercial prototype to laboratory instrumentation. Finally, these sensors employ a wide range of sophistication in both the laser source and associated analytical spectroscopy. In the ultimate applications, however, many attributes of the sensors are in common, such as the need for robust operation and hardening for harsh industrial environments.

2. LASER-BASED SENSOR FOR STEELMAKING

The majority of steel produced today in North America employs the basic oxygen steelmaking process. Oxygen injected into the melt at high velocities is used to convert molten iron to steel in a refractory-lined basic oxygen furnace (BOF) by oxidizing carbon to carbon monoxide.[1] The current industry practice relies on a static materials-and-energy-balance model to calculate the quantity of oxygen required to convert the reactants into steel. Uncertainties in the chemical composition of the starting material, such as recycled steel scrap, and the dynamics of the conversion process during oxygen blowing lead to undesirable variations in the final carbon content and temperature of the steel, and underline the need for real-time sensors to aid in process control. Further complexities in the process are created by the use of post-combustion technology during oxygen blowing.[2,3] While this technology offers an increase in steelmaking efficiency, care must be taken to extract the maximum amount of thermal energy from the CO-rich furnace off-gas without overheating furnace refractory linings.

Sandia is developing an optical sensor based on mid-infrared tunable diode lasers (TDLs) to provide real-time information on both the temperature and composition of the off-gas emanating from the basic oxygen furnace (BOF) during the oxygen blow.[4] This technique is a non-invasive optical method employing robust, low-maintenance hardware. Other techniques being developed to monitor relative CO and CO_2 concentrations involve an extractive measurement using mass spectrometry and an optical emission technique.[5] Extractive measurements suffer from a significant time delay for process control purposes and the maintenance associated with an extractive gas probe in the hostile off-gas environment. Optical emission methods, on the other hand, are limited by low spectral resolution and the optical thickness of the infrared emitting gases.

Part of the SPIE Conference on Advanced Sensors and Monitors for Process Industries and the Environment
Boston, Massachusetts • November 1998 SPIE Vol. 3535 • 0277-786X/99/$10.00

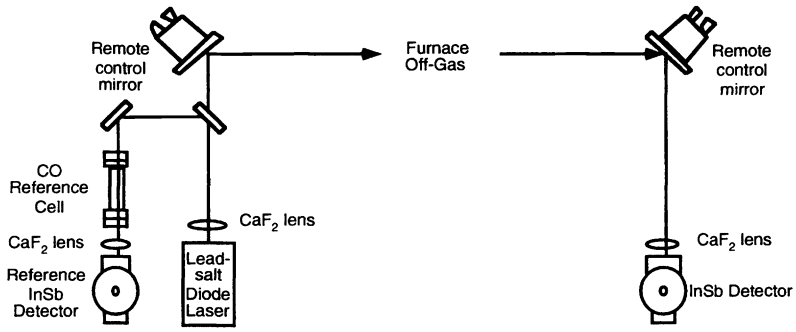

Figure 1. Experimental layout of infrared TDL absorption sensor for CO and CO_2 measurement in BOF offgas streams.

We anticipate that real-time data from the TDL-based sensor along an optical line-of-sight will be useful in defining optimum process parameters such as: oxygen flow rate to primary and post-combustion lance orifices; oxygen-lance position relative to the molten bath height; and total oxygen blowing time. An additional goal is the correlation of sensor signals with the carbon content and temperature of the steel bath at the end of the blow.

An optical sensor based on infrared absorption spectroscopy is shown in Figure 1. The optical hardware consists of transmitter and detector modules. The infrared light source is a tunable semiconductor laser diode operating in the 2200-1900 cm^{-1} wavenumber region at a temperature of 80 to 120K. Coarse wavelength tuning is achieved by adjusting the laser temperature, while fine wavelength tuning is accomplished by varying the diode injection current.

The laser output is collimated and directed toward a remotely controlled output mirror. A small fraction of the TDL beam is reflected from a beamsplitter in the transmitter module through a gas cell containing low-pressure carbon monoxide. The resulting CO absorption spectrum is measured by a reference detector and is used to monitor and ensure stable laser operation. The output beam from the transmitter module is steered through the hot, furnace off-gas toward the detector module (also shown in Figure 1). Signals from both sample and reference detectors are digitized and processed by a remotely-located, microprocessor-based data acquisition system.

Transmitter and detector modules are mounted on platforms on opposite sides of the basic oxygen furnace, shielded by heat shields. A visible laser beam is overlapped with the TDL beam in the transmitter module (not shown in Figure 1). Following installation, optical alignment of transmitter and detector modules is easily accomplished using the red laser beam as a guide. We have made measurements in both pilot-scale and full-scale BOF shops. The pilot-scale facility at Bethlehem Steel's Homer Research facility (Bethlehem, PA) can hold up to 2 tons of steel and has a 0.36-m (14-inch) absorbing pathlength. Full-scale measurements have been made at Bethlehem Steel's Sparrows Point facility (Baltimore MD); the #1 furnace has a 280-ton capacity and a mouth diameter of 3.65 m (12 feet). The total laser pathlength in this commercial facility, from the transmitter to the receiver, is approximately 11 m.

The optical sensor has been designed for operation in the harsh, industrial environment. The footprints of the transmitter and detector modules are 2 x 2 feet square and 1 x 1.5 feet square, respectively. Hermetically-sealed optical enclosures with purged windows are used to maintain a dust-free environment in the two modules. Water-jacketed enclosures provide robust, maintenance-free cooling for the transmitter and detector modules.

The sensor signal takes the form of an absorption spectrum for CO and CO_2 that is generated as the diode laser is scanned through its wavelength tuning range. Absorption spectra at two different regions of the mid-infrared spectrum are illustrated in Figs. 2 and 3. The spectral region presented in Fig. 2 is appropriate for the pilot-scale BOF, but these CO absorption features are optically thick under the conditions of a full-scale furnace due to the much longer pathlength. In both figures, the relative intensities of the absorption features are strongly dependent on the off-gas temperature along the optical line-of-sight. Calibration spectra along with computer models are used to determine the average off-gas temperature in real-time. Relative concentrations of CO and CO_2 are monitored using absorption line intensities for the two species.

The duration of a steelmaking oxygen blow is approximately 20 to 25 minutes. Typically, a commercial furnace uses 300 tons combined weight of molten iron, recycled steel and slag, and an oxygen flow rate of 20,000 scfm. The mass loading of particulates in the furnace off-gas stream is approximately 40 lbs per ton of steel produced.

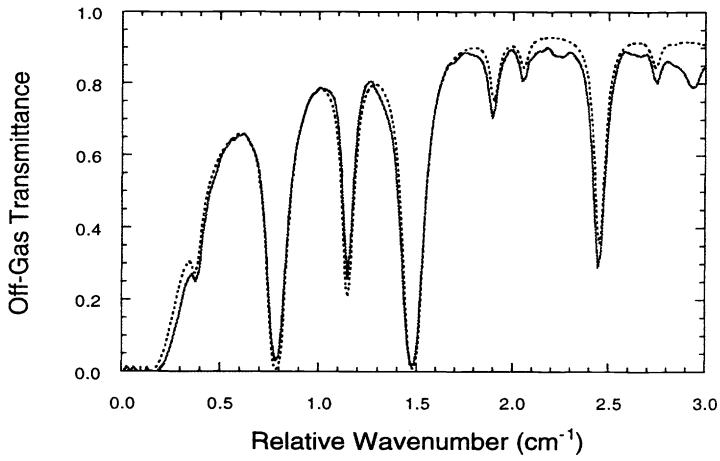

Figure 2. Gas-phase absorption spectrum during BOF oxygen blowing (solid), and calculated CO transmittance (dashed) for an average gas temperature of 1450 K (2150°F), CO concentration 49%, and absorbing path length of 0.36 meters (14 in.).

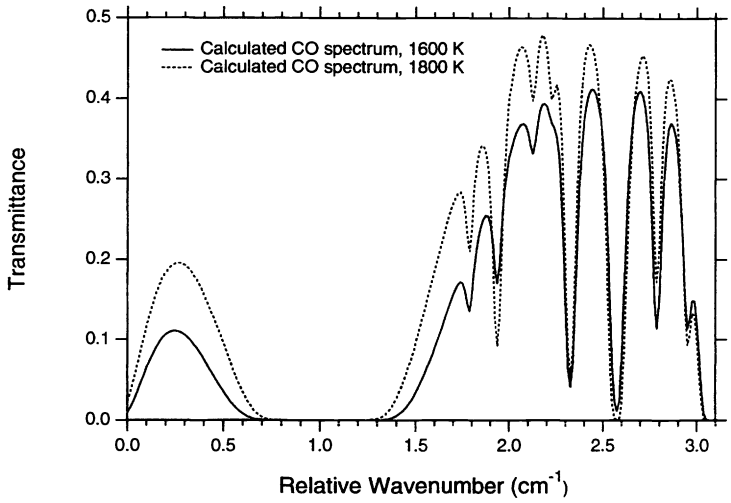

Figure 3. Calculated transmittance spectra for CO at a concentration of 50%, path length of 3.65 meters (12 ft), and 1600 and 1800 K (2420 and 2780°F), solid and dashed curves,

The TDL beam is strongly attenuated by particles and gases due to the long pathlength through the off-gas in the full-scale furnace. The transmitted TDL beam intensity is therefore extremely small, and is difficult to detect in the presence of the very large amount of infrared emission from hot particles and gases. In order to efficiently detect the laser beam under these conditions, we incorporate the standard TDL technique of frequency modulation at 50 kHz, followed by demodulation at 100 KHz. This allows us to electronically filter out the unwanted background emission, which, although time-varying, is not amplified by the lock-in. We refer to this second-harmonic spectrum as the "2f" spectrum.

To select the optimal wavelength region for measurements at the full-scale furnace, we first determine wavelength ranges in which our infrared laser beam is not totally absorbed by the off-gas. Transmission spectra are calculated for off-gas path lengths of 3.65 m, CO concentration of 50%, and temperatures in the range of 1600 to 2200 K. An example is shown in Figure 3 that compares CO transmittance for temperatures of 1600 and 1800 K in a different spectral region than plotted in Figure 2. From this example it is clear that some features of the CO absorption spectrum are completely absorbing under the expected operating conditions. Other features have very different temperature dependences and can be used for the determination of off-gas temperature. Interpretation of experimental measurements is complicated, however, by our method of signal processing. The wavelength modulation / demodulation technique used to enhance signal detection also alters the shape of the individual absorption line profiles, and this must be accounted for when quantitatively analyzing the sensor data. Accordingly, we have formulated a computer algorithm for transforming experimental and calculated transmission spectra into 2f spectra.

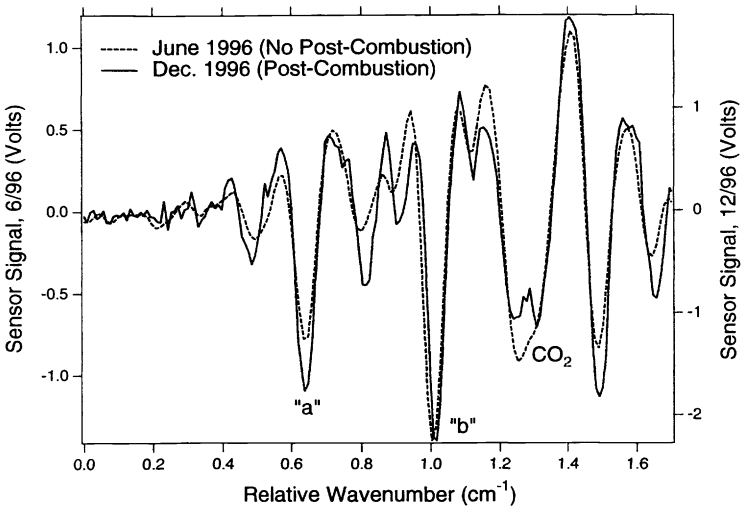

Figure 4. Time-averaged sensor signals of off-gas during and oxygen blow before (dashed curve) and after (solid curve) the incorporation of a post-combustion oxygen lance in the full-scale BOF at Sparrows Point. CO features labeled "a" and "b" are used to extract off-gas temperatures. Feature labeled "CO_2" at 1.3 cm^{-1} is due to CO_2.

Figure 4 shows a sensor 2f signal obtained mid-way during the oxygen blow for a heat in June 1996 (dashed curve). This curve was produced by averaging individual laser scans over a period of 4 seconds. Many of the strong absorption features agree well with a calculated CO spectrum for 1800 K, and are consistent with industrial operating conditions and other attempts to measure gas temperatures.[6]

Following measurements in June 1996, an oxygen lance modified for post-combustion operation was put into service at Sparrows Point. This procedure introduces additional oxygen into the CO-rich gas near the top of the furnace with subsequent combustion and the formation of additional CO_2. Consequently, we anticipated optical measurements showing an increased amount of CO_2 and higher off-gas temperatures compared to our earlier data. This is also illustrated in Figure 4 for a sensor signal obtained during December 1996 (solid curve) and compared to the experimental data from June 1996 (dashed curve). The relative intensities of the CO features labeled "a" and "b" indicate that the off-gas temperature has increased by as much as 100 K to 1900K following the installation of post-combustion lance technology. Furthermore, the two overlapped absorption features at 1.2 and 1.3 cm^{-1} relative-wavenumber are due to CO and CO_2, respectively. The CO feature has decreased in intensity for the post-combustion measurement (solid curve), while a stronger and more clearly resolved feature due to additional CO_2 is present in the furnace off-gas as labeled.

Off-gas temperatures are extracted from the ratio of these absorption intensities using a computer model, and are plotted for the latter half of an oxygen blow (Figure 5). The off-gas temperature increases slowly during this period from a value of 1910 to 1960 K. Individual data points represent a three-second instrument response time. The temperature plot is truncated before the end of the oxygen blow due to decreasing CO concentration during the final stage of decarburization.

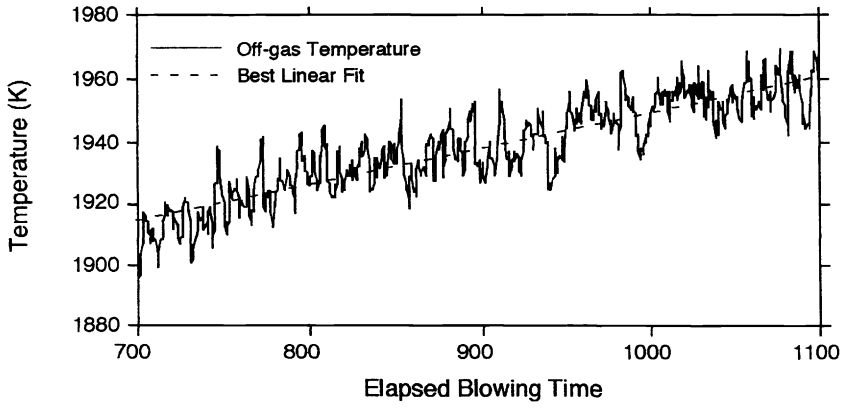

Figure 5. Off-gas temperature measured during oxygen blowing in the full-scale BOF, using intensities of CO absorption features marked "a" and "b" in Figure 4.

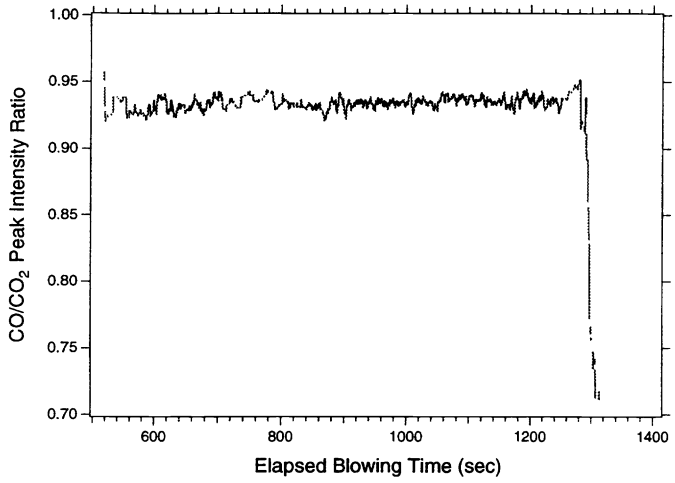

Figure 6. Off-gas CO/CO_2 ratio tracked during oxygen blowing in the full-scale BOF, using intensities of CO and CO_2 absorption features marked "a" and "CO_2" in Figure 4.

By using the intensities of the absorption features labeled "a" and "CO_2" in Figure 4, the relative concentrations of CO and CO_2 in the furnace off-gas can be tracked in real-time. This is illustrated in Figure 6, showing a sharp drop in CO concentration near the end of melt decarburization.

Two extended series of measurements have been made with the laser-based sensor at Sparrows Point during fall 1997 and spring 1998. Data for more than 600 heats have been analyzed in order to extract trends in off-gas temperature and composition as a function of blowing time. We have used these measurements to develop a statistically significant set of sensor data for correlation with process data. We find that we are able to predict the final melt temperature with an accuracy of ±17K, and the final melt carbon content with an accuracy of ±0.005%. The ability of our TDL-based sensor to achieve these accuracies is of great interest to the steel industry. In future work we will evaluate the most effective means of incorporating the real-time sensor signals into an improved process control scheme for basic oxygen steelmaking. We are also evaluating the use of the TDL sensor for electric arc steelmaking, for the purpose of CO/CO_2 concentration and off-gas temperature quantification. These quantities are important for efficient post-combustion in this energy-intensive manufacturing process.

3. LASER-INDUCED BREAKDOWN SPECTROSCOPY MONITOR

A program was initiated at Sandia to develop and demonstrate an advanced continuous emissions monitor (CEM) that will provide real-time measurement of hazardous metal emissions in the waste streams of thermal treatment facilities.[7] In such facilities (e.g. incinerators or confined burn facilities), the fate of metals is a complex phenomenon controlled by mechanisms such as particle entrainment, chemical interactions, vaporization, condensation, particle coagulation, and particle collection by air pollution control system (APCS) devices. Important parameters include the volatility of metal species and the treatment process time and temperature profiles. As the combustion products cool downstream of the primary reactor, vaporized metals are expected to nucleate homogeneously or condense onto other particles. Homogeneous nucleation typically produces sub-micron-sized particles, while heterogeneous condensation favors enrichment of metals onto the smallest particles due to their higher surface-area-to-mass ratios. For accurate and reliable operation, a metals CEM must respond over a wide range of waste stream conditions, which may include vapor phase species and highly variable metal particulate loadings.

The technologies in the forefront of the development of CEMs for metal species include inductively coupled plasma atomic emission spectroscopy (ICP/AES),[8] microwave-induced plasma atomic emission spectroscopy (MIP/AES), and laser-induced breakdown spectroscopy (LIBS).[9] For on-line metals analysis, Sandia has chosen to pursue LIBS, which is the only technology that has been demonstrated in the field as an *in-situ*, noninvasive, real-time diagnostic.

LIBS is an atomic emission spectroscopy diagnostic that utilizes a pulsed laser beam as the excitation source. The laser beam is tightly focussed in a particle source flow. The resulting optical breakdown, also referred to as a laser-induced plasma or

laser spark, dissociates molecules and excites all atoms within the plasma volume. In addition to the broadband emission of the plasma, the excited atoms relax, producing radiation at characteristic frequencies. This enables determination of elemental composition. Because the laser-induced plasma dissociates all species into single atoms, no molecular information is obtained. However, an advantage of LIBS as a total metals monitor is that the LIBS technique provides a signal that is directly proportional to the total concentration of metal species. Specific applications of LIBS for the analysis of aerosols include a number of metal species such as beryllium, lead and mercury.[10-12]

A LIBS-based metals monitor is well suited for quantitative analysis over a large dynamic range. Of further significance, the *in-situ* nature of a LIBS monitor eliminates the need to extract a sample from the effluent stream. When such samples are extracted, they are prone to variable losses in the sampling line. These losses depend on the particulate loading in the effluent stream. Sample lines may also contribute to considerable hysteresis in the measured concentrations due to contamination.

The Sandia LIBS instrument utilizes a 1064-nm Nd:YAG laser as the excitation source, with a nominal pulse width of 10 nsec and pulse energy of 400 mJ. A schematic of the LIBS monitor system is presented in Figure 7. After beam expansion to 12 mm, the plasma is created using a 75-mm focal length, 50-mm diameter, UV-grade lens. These parameters are adequate to assure that breakdown is initiated with each laser pulse. The focusing lens also collects the plasma emission, which is launched into a fiber optic bundle and coupled to a 0.25-m spectrometer and time-gated, intensified CCD detector array.

While the Sandia LIBS instrument has been field tested at a number of different sites, in this paper we focus on a recent series of demilitarization experiments performed under the auspices of the Industrial Operations Command, Demilitarization Technology Office.[12] Lockheed Martin and the Naval Air Warfare Center (NAWC) are developing a procedure for demilitarization of the Shillelagh Anti-Tank Missile. In this process, the rocket motor is mounted in the wall of a sealed chamber (Total Containment Vessel, TCV) and ignited. During burning, the rocket emissions are entirely contained in the chamber. After completion of combustion, the motor exhaust gases are ducted to treatment equipment where constituents unsuitable for discharge are removed prior to venting to atmosphere. A number of toxic gases, chemicals, and Resource Recovery Act (RCRA) listed hazardous metals are generated in the Shillelagh burn tests. The primary goal of the TCV tests was to provide the data to develop a prototype Shillelagh disposal facility and, subsequently, a full-sized facility scaled to dispose of as many as 100 Shillelaghs per day.

The predominant RCRA metal of interest is lead because the solid propellant in the Shillelagh contains 32 grams of lead. A the particulate filtration system was positioned following the test chamber, and the Sandia LIBS system measured, *in situ*, the concentration of lead before the exhaust gas reached this system. As much as 10 grams of airborne lead (test-time integrated) was measured using the LIBS system during one of the tests, implying the balance (67%) of the lead remained in the containment vessel. The particle-laden gases passed through a set of filters designed to remove particles with 99.99999% efficiency. The concentration of lead after this scrubber system was measured by first extracting a sample from the exhaust stack, then introducing it into an inductively coupled (ICP) spectrometer, where the atomic emission lines for lead were monitored and recorded.[8] The lower detection limit of the ICP system was 2 $\mu g/m^3$. For these tests the lead concentration following the scrubber system was below the detection limit of the ICP system.

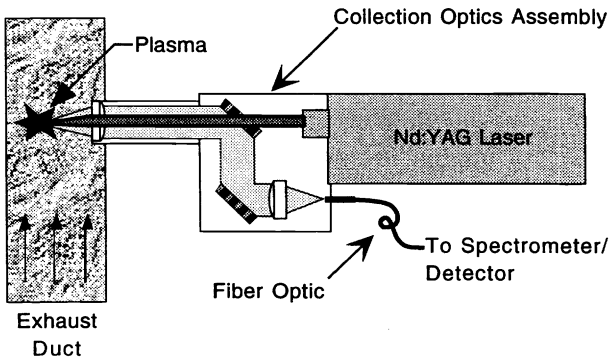

Figure 7. Schematic of LIBS monitor system probe.

To make these measurements, data were collected using a 5.0 Hz laser pulse rate and ensemble averaging of 150-shot sequences. After each 150-shot sequence, the lead concentration was calculated and saved to disk along with the spectral data, a procedure that takes 3 seconds. Accordingly, a 30-s average lead concentration value was recorded every 33 seconds. The spectral data generated by the LIBS technique is characterized by a continuous background emission signal with superimposed discrete atomic emission line signals. The 405.8-nm atomic emission line was used for analysis of all lead emissions data for this test series.

For each targeted analyte emission line, a LIBS signal is calculated based on the integrated emission intensity of the atomic emission line peak normalized by the integrated intensity of the continuum background in an adjacent spectral region. The continuum background is calculated as the average intensity of discrete bandwidths on each side of the analyte emission line. For the TCV test series, the 405.8-nm lead line was integrated over a spectral bandwidth of 2 nm. The background intensity was calculated over bandwidths of 1.5 nm centered at 400.5 and 409 nm. The LIBS calibration curve was calculated using a linear least-squares fit of the LIBS signal (i.e. integrated peak normalized to continuum baseline) as a function of known analyte concentration. The calibration curve was generated in the laboratory over the range of 500 to 2000 micrograms of lead per actual cubic meter (µg/acm), utilizing a calibration flow stream of known mass concentration. The calibration was performed using the identical LIBS parameters (e.g. lens focal length, laser power, and detector integration time) as used for the field measurements.

The lead concentration data are reported as a function of delay time with respect to the firing of the Shillelagh motor at t=0 seconds. At 300 seconds, positive pressure was vented from the tank through the 10-inch exhaust duct. From 390 seconds on, the TCV was continually flushed by drawing through ambient air at a rate of approximately 1500 scfm until t = +1020 seconds.

The time-resolved lead concentration data are presented in Figure 8A for the TCV-4 through TCV-7 tests. The lead emission profiles are similar for all four Shillelagh shots. The lead concentration values display a rapid rise as the positive pressure is vented at t = +300 seconds to values between 30,000 and 40,000 µg/acm. The lead concentrations then decrease slightly until the blower initiation at t = +390 seconds, when they were observed to rapidly increase to their maximum values in the range of 40,000 to 60,000 µg/acm. When the blower and purge flow were initiated at 390 seconds, the lead concentration levels were observed to decrease steadily, and reached a final value of about 1000 µg/acm when the tank was again sealed. Once the tank was sealed, the lead concentration level remaining in the 10-inch duct was on the order of 500 µg/acm. This residual lead trapped in the duct was observed to decay at a rate of about 50 µg/acm per minute. The time-resolved lead data are presented in Figure 8B at an expanded scale over the last four hundred seconds of the test.

The maximum lead concentration levels measured in the exhaust duct are summarized in Table 1 for four tests. In addition, the LIBS data were averaged over the test period (t = 300 to 1020 seconds) to produce the average lead concentration levels shown in Table 1 for comparison to extracted samples and gravimetric analysis. Extracted samples by definition provide an average concentration value based on the total collected mass and volume of sampled gas. The maximum and average lead

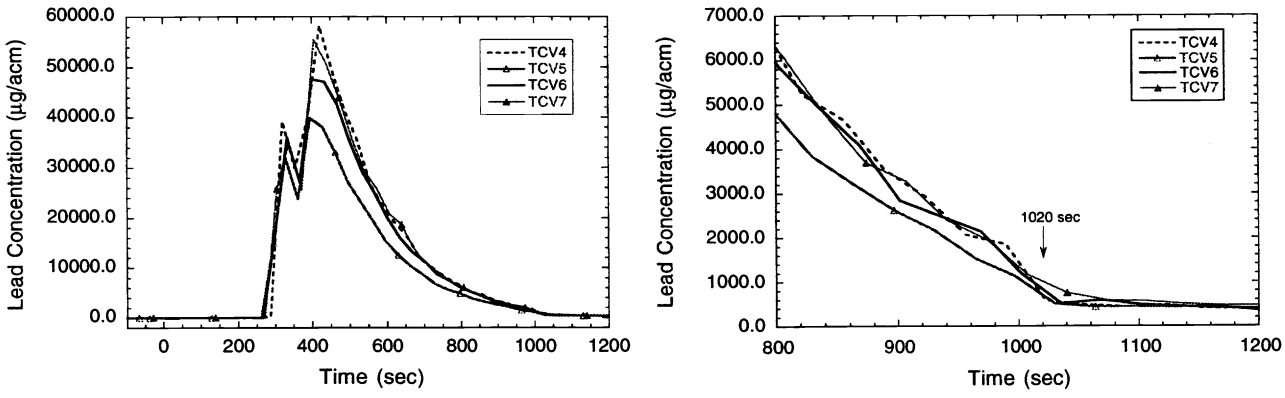

Figures 8A (left) and 8B (right). Lead concentration values in 10-inch exhaust duct measured by LIBS monitor during the TCV test series.

Table 1. Lead concentration values, before particulate scrubber, measured by LIBS. Time-integrated values are estimates from Reference 13.

	TCV-4	TCV-5	TCV-6	TCV-7
Average (μg/acm)	20,700	15,000	18,500	19,600
Maximum (μg/acm)	58,200	39,900	47,600	55,500
Time-integrated (μg)	10146793	6798281	9596306	9849817

concentration values of the LIBS data correlate with one another for the four tests, and range from 58,200 and 20,700 μg/acm, maximum and average values, respectively, for TCV-4; to 39,900 and 15,000 μg/acm, respectively, for TCV-5. The average lead concentrations as measured with extractive sampling ranged from 23,000 to 33,900 μg/acm of sampled gas.[13] The average LIBS lead concentration data ranged from 20 to 56% less than the extractive sampling results for the TCV test series. For the four tests, the LIBS-based concentration values averaged 36.5% less than the lead concentration data determined with extractive sampling. The overall agreement between the two techniques is very good, given that no analysis was performed to normalize the two data sets to account for any differences in gas sample volumes resulting from temperature and water vapor changes. The estimated (worst case efficiency) time-integrated lead concentrations after the scrubber system for all tests is 1107 μg, which represents the detection limit of the ICP CEM.[8] The action level (OSHA) for lead is 50 μg/acm for an 8-hour work day.[14]

In summary, the Sandia LIBS system was successful in providing real-time monitoring of lead emissions during the test series. The estimated uncertainty for the lead concentration measurements is ±30 μg/acm, with a minimum detection level of 60 μg/acm. The *in situ* configuration of the LIBS system was advantageous in view of the wide dynamic range of lead concentrations encountered in the TCV test series. Overall, the utility of a continuous emissions monitor in providing time-resolved emissions data was demonstrated. A better understanding of peak concentration levels and decay times will be useful for further process optimization with regard to system turnaround times, rocket destruction rates, the effects of cumulative rocket firing, and in the design of air pollution control equipment.

4. LASER-BASED INFRARED IMAGING FOR EVALUATION OF SURFACE CLEANLINESS

Sandia is currently developing a real-time, laser-based method to provide both qualitative and quantitative assessments of surface cleanliness for a wide variety of applications. The availability of a convenient analysis technology for on-site, post-cleaning determination of surface contamination allows more rapid and accurate assessments of the efficiency of a given cleaning technique. The development of an on-line technique will remove the need for remote analysis and the need to send process parts out to a separate laboratory, thereby eliminating processing delays. The information provided by this new optical method will assist the process operator in determining subsequent actions to be taken, as well as aid in distinguishing between specific contaminants. Overall, this will lead to improved alternative cleaning products and processes, and to the reduction of hazardous materials usage and handling.

Currently, the detection of surface contaminants on reflective surfaces is most conveniently and rapidly done by Fourier transform infrared (FTIR) reflectance methods.[15, 16] These non-destructive, non-contacting optical techniques identify the chemical constituents of the contaminants, and can yield quantitative measurements with appropriate calibration. Infrared optical methods are particularly useful for cleanliness analysis since the surface is probed under ambient conditions. As a result, the method is amenable to on-line usage, although insensitive to the sub-monolayer quantities detectable by various high-vacuum electron and ion spectroscopic techniques (X-ray photoelectron spectroscopy, Auger electron spectroscopy, and secondary-ion mass spectrometry).

A highly desirable characteristic of a cleaning verification instrument is the ability to rapidly survey large surface areas and to determine the location and extent of any remaining contaminant following cleaning operations. The laser-based instrument under development offers this capability for hydrocarbon species that possess infrared absorption bands in the 3-μm wavelength region. While an FTIR-based infrared reflectance analysis is able to characterize a very broad range of organic

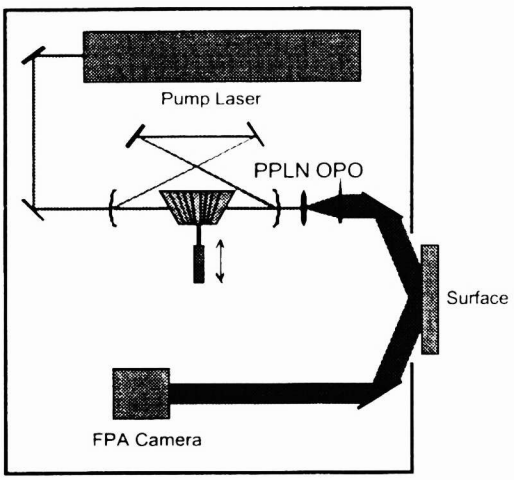

Figure 9. PPLN/OPO imaging surface analysis system.

constituents and many inorganic species, a surface-probing FTIR instrument measures a spectrum at only a single small area on a sample, thus requiring broad area surveys to be done by sequentially probing many points. The rate of measurement by an FTIR is constrained by the relatively low spectral brightness (compared to a laser) of the incandescent illumination sources used in an FTIR instrument. This makes it necessary to use relatively long integration times to achieve an acceptable signal-to-noise ratio.

Alternately, Sandia's new surface analysis technique involves an imaging system that employs a widely tunable infrared laser in conjunction with an infrared camera (see Figure 9) for surveying contamination levels over large surface areas in a real-time imaging mode. The laser and imaging system were adapted for this application from a device that was developed previously for gas leak detection.[17, 18] The laser is broadly tunable over the 1.3-4.5 μm wavelength range, thus allowing the detection of many hydrocarbon contaminants via their CH-, OH-, and NH-stretch absorptions. The potential for extending the laser tunability into the long-wave infrared spectral region (>5 μm) is also being explored as part of this project, and may extend the capabilities of the real-time imaging instrument to the detection of a very broad range of organic, and some inorganic, molecular species.

Real-time imaging of a broad surface area as it is illuminated by a high-brightness infrared laser allows a single-wavelength reflectance measurement of ~65,000 surface points to be made on a timescale of 1/30th of a second. Measurements at multiple wavelengths are made by tuning the laser and repeating the image acquisition at each desired wavelength. While a detailed spectral map of a surface can be generated over the laser tuning range, the primary intent of the system is to provide for rapid areal surveys at a few key wavelengths that are indicative of expected contaminants.

An important advance that makes this surface analysis tool possible is the application of quasi-phasematching (QPM) to infrared lasers. For example, continuous-wave optical parametric oscillators (OPOs) employing the QPM material periodically-poled lithium niobate (PPLN), are capable of tuning over the full 1.3-4.5 μm spectral region while emitting more than 0.5 W of power. The current tuning range of the PPLN-based laser is limited at long wavelengths to about 4.5 μm, and thus limits the sensitivity of the chemical imaging system primarily to functional groups containing hydrogen atoms (C-H, N-H, O-H). While this wavelength range is generally useful for the detection of most common hydrocarbon contaminants, extension of the laser tuning range beyond 5-μm wavelength is highly desirable to identify other molecular species (such as silicones and inorganics), as well as to afford specific identification of hydrocarbon molecular species.

Initial work at Sandia has demonstrated the feasibility of detecting hydrocarbon species on metallic surfaces by this method. The laser system is described in more detail elsewhere.[19] Briefly, the pump source is a pulsed (30 Hz), injection-seeded Nd:YAG. A portion of the 1.064 μm output radiation is frequency-doubled and used to pump a dye laser, which lases near 800 nm. The tunable output of the dye laser is mixed with an additional portion of the Nd:YAG fundamental radiation in an uncoated LiNbO3 DFG crystal to produce a difference-frequency beam that is tunable from ~3.1 to 3.5 μm wavelength. This infrared radiation is subsequently amplified by mixing with the remaining 150 mJ of 1.064 μm fundamental radiation in the OPA crystal (identical to the DFG crystal). The OPA output energy at 3.3 μm is 4.5 mJ. The mid-infrared output of this DFG/OPA laser can be rapidly tuned between two frequencies with a switching time of <33 msec. This is accomplished

using a piezo-electric translator (PZT) attached to the dye laser grating arm. The PZT deflects the grating arm up to a maximum displacement of 100 μm, which tunes the dye laser frequency as much as 25 cm^{-1}. Both the DFG and OPA crystals are mounted on galvanometers, which allow their respective phasematching angles to be tuned synchronously with the grating tuning.

In the demonstration experiments, an aluminum plate, approximately 6 by 6 inches, is illuminated with the above laser radiation at 2830 and 2805 cm^{-1}, respectively, and is imaged by a 256 x 256 InSb focal plane array camera (Amber). The laser is rapidly tuned between the two illumination frequencies at a rate of 30 Hz, and a real-time video image is created showing the presence of highly absorbing organic layers on the metal surface. Two solvents were deposited on the plate, methanol on the left and d-limonene (a naturally occurring terpene that is of interest as an environmentally benign solvent for cleaning operations) on the right. The on-line nature of these measurements allows the visualization of the evaporation, solvation and transport of d-limonene by methanol. The first two images shown in Figure 10 are successive frames at the two laser frequencies. The intensities of the reflected light from the aluminum substrate were normalized during post-processing of both images to permit comparison of absorbing features. Both hydrocarbons absorb strongly at 2830 cm^{-1} in the image on the left in Figure 10 and are easily detectable, appearing uniformly black. However, by selecting a second laser illumination wavelength at 2805 cm^{-1}, small differences in the absorptive properties of the two solvents are visible, as seen in the image in the center in Figure 10.

Less highly absorbing portions of the hydrocarbon solvents in the image are located primarily around the edges and the top of the d-limonene feature. This difference in the observed reflectance is substantiated by the spectral absorption properties of the two hydrocarbon solvents, presented in Fig.11. A substantial relative difference in absorption coefficients is obtained for the two solvents at the two different laser illuminations. The natural logarithm of the ratio of the two images (the images recorded at 2830 and 2805 cm^{-1}) is displayed in the right image of Fig. 10.

These results demonstrate the feasibility of real-time detection of hydrocarbon species on reflective surfaces using infrared-laser illumination. Film thickness of the two solvents in these experiments were estimated to be several micrometers and rendered the two hydrocarbons easily detectable using near-normal reflectance, although the spectral contrast between the two solvents is minimized for these thick films. In future work, we will increase the sensitivity of such measurements for very thin hydrocarbon residues by employing grazing-angle reflectance geometry. Furthermore, the discrimination between different condensed-phase materials will be possible by a careful choice of multiple laser illumination frequencies, and will also be easier to observe for less highly absorbing thin films.

Figure 10. Illumination by a tunable infrared laser at 2830 (left image) and 2805 cm^{-1} (center image) of two hydrocarbon solvents on a reflective aluminum plate. Methanol and d-limonene appear as absorbing features on the left and right, respectively, of each image. Image on the right is a false-color intensity ratio.

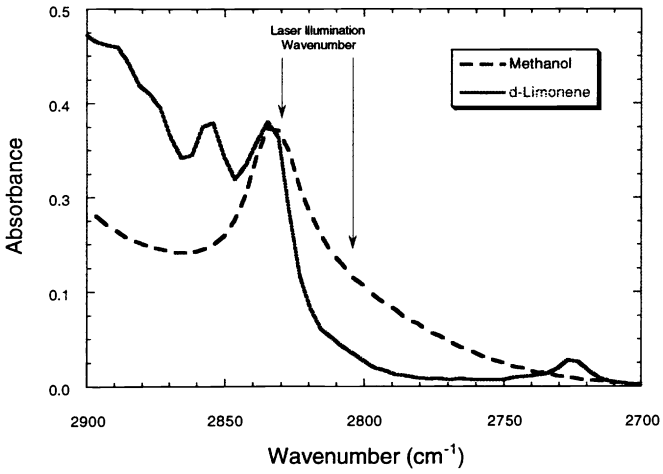

Figure 11. Spectral absorbance for methanol and d-limonene. Laser illumination frequencies are indicated by the two arrows at 2830 and 2805 cm^{-1}.

We are in the process of extending these feasibility experiments by incorporating the PPLN/OPO laser system used in the raster-scanned gas imager[19, 20] that will allow us to interrogate the surface sample at a series of different wavelengths. In addition, we have incorporated microscope optics for illumination of the surface, which enable high-resolution (2μm per pixel) images of surface contamination to be rapidly acquired. Finally, quantitative applications of the technique for cleanliness evaluation require the calibration and rapid, statistical analysis of infrared images at multiple wavelengths, and become particularly important for on-line processing applications. Analytical methods, such as chemometrics, will be incorporated into the final sensor for the purpose of contaminant speciation in the real-time imaging mode of operation.

ACKNOWLEDGMENTS

This paper describes the work of numerous Sandians. The authors are please to acknowledge the contributions of Steven Buckley, Don Hardesty, Howard Hirano, Howard Johnsen, Joel Lipkin, Peter Ludowise, James Ross, and Jim Wang. Financial and programmatic support are gratefully acknowledged from the American Iron and Steel Institute; the U.S. Department of Energy's Offices of Industrial Technology, Technology Development/CMST-CP, and Fossil Energy; the U.S. Department of Defense's Office of Munitions, and the Gas Research Institute.

REFERENCES

1. W.T. Lankford, Jr., N.L. Samways, R.F. Craven, H.E. McGannon, *The Making, Shaping, and Treating of Steel, 10th Edition*, Chapter 16: Oxygen Steelmaking Processes, Herberk and Held, Pittsburgh (1985).
2. G.J. McManus, "Electric Furnace Post Combustion Takes Off," *Iron & Steel Engineer*, **72** (4), pp. 90-91 (1995).
3. F. A. Vonesh, Jr., and N. G. Perrin, "Post-Combustion for the Electric Arc Furnace," *Iron & Steel Engineer*, **72** (6), pp. 30-32 (1995).
4. S.W. Allendorf, D.K. Ottesen, D.R. Hardesty, D. Goldstein, C.W. Smith, and A.P. Malcolmson, "Laser-based sensor for real-time measurement of offgas composition and temperature in BOF steelmaking," *Iron and Steel Engineer*, **75** (4), pp. 31-35 (1998).
5. G.J. McManus, "Post Combustion Stirs Broad Interest," *Iron and Steel Engineer*, **73** (11), pp. 53 (1996).
6. W. Hutchinson, Bethlehem Steel Corporation, private communication, March 1997.
7. D.W. Hahn, W.L. Flower, and K.R. Hencken, "Discrete particle-detection and metal emissions monitoring using laser-induced breakdown spectroscopy," *Appl. Spectrosc.* **51** (12), pp. 1836-1855 (1997).
8. M.D. Seltzer and G.A. Meyer, "Inductively-coupled argon plasma continuous emissions monitor for hazardous air pollutant metals," *Environ. Sci. & Tech.* **31** (9), pp. 2665-2672 (1997).

9. D.A. Cremers and L.J. Radziemski, *Laser Spectroscopy and Its Applications,* Chap. 5: "Laser Plasmas for Chemical Analysis," Marcel Dekker, New York (1987).
10. J.P. Singh, H. Zhang, F.Y. Yueh, and K.P. Carney, "Investigation of the effects of atmospheric conditions on the quantification of metal-hydrides using laser-induced breakdown spectroscopy," *Appl. Spectrosc.* **50** (6), pp. 764-773 (1996).
11. S. Yalcin, D.R. Crosley, G.P. Smith, and G.W. Faris, "Spectroscopic characterization of laser-produced plasmas for in-situ toxic metal monitoring," *Haz. Waste Haz. Mater.* **13** (1), 51-61 (1996).
12. D.W. Hahn, "Laser-induced breakdown spectroscopy for sizing and elemental analysis of discrete aerosol-particles," *Applied Phys. Letters*, **72** (23), pp. 2960-2962 (1998).
13. E. Erickson, "Shillelagh Total Containment Vessel Tests 4-7 Data Summary and Analysis Report," Lockheed Martin Missiles and Space and Naval Air Warfare Center Weapons Division (1998).
14. OSHA: 29 CFR 1910.1025
15. D. Ottesen, "Detection of contaminants in steel tubing using infrared reflection spectroscopy," *in Proceedings of SPIE, Optical Techniques for Industrial Inspection*, Vol. 665, G. Cielo, ed., (Society of Photo-Optical Instrumentation Engineers, Bellingham, WA, 1986), Quebec City, Canada, pp. 226-233.
16. D. Ottesen, "An experimental and theoretical study of the infrared reflectance of thin oxide films on metals," J. *Electrochem. Soc.,* **132** (9), pp. 2250-2257 (1985).
17. P.E. Powers, T.J. Kulp, and "Differential backscatter absorption gas imaging," *Proceedings of SPIE, Infrared Technology and Applications XXIII*, Vol. 3061, (Society of Photo-Optical Instrumentation Engineers, Bellingham, WA, 1997), Orlando, FL, pp. 265-268.
18. T.J. Kulp, P.E. Powers, R. Kennedy, and U.B. Goers, "The development of a pulsed backscatter absorption gas imaging (BAGI) system and its application to the visualization of natural gas leaks," submitted for publication to *Applied Optics*, September, 1997.
19. T.J. Kulp, P.E. Powers, and R. Kennedy, "The development of a laser-illuminated infrared imager for natural gas leak detection," in *Proceedings of the U.S. Department of Energy Natural Gas Conference*, Houston TX, March 24-27, 1997, paper 2.7.
20. L.E. Myers, R.C. Eckardt, M.M. Fejer, R.L. Beyer, and W.R. Bosenberg, "Multigrating Quasi-Phase-Matched Optical Parametric Oscillator in Periodically Poled $LiNbO_3$," *Optics Letters* **21**, pp. 591-593 (1996).